Design and Implementation of an Intelligent Grid Interfaced Solar Water Pumping System for Sustainable Agriculture

Dennai Mohammed Yassine[1*], Tedjini Hamza[1]

[1] Laboratory of Smart Grids & Renewable Energies (S.G.R.E), Faculty of Technology, Department of Electrical Engineering, Tahri Mohamed University Bechar, B.P 417, 08000, Algeria.

Author Correspondence email: **dennai.mohammedyassine@univ-bechar.dz**

Received: 04/ 2023; **Accepted:** 07/2023; **Published:** 08/ 2023

Abstract:

This research paper presents developing and implementing an Intelligent Grid Interfaced Solar Water Pumping System for Sustainable Agriculture, incorporating an Adaptive Neuro-Fuzzy Inference System (ANFIS) based Maximum Power Point Tracking (MPPT) algorithm. The primary objective is to enhance agricultural practices' energy efficiency and sustainability by efficiently harnessing solar energy for water-pumping applications. The ANFIS current-voltage controlled MPPT algorithm demonstrates remarkable adaptability and accuracy in tracking the solar photovoltaic array's maximum power point, optimizing energy extraction. Integration with the power grid allows surplus solar energy injection, reducing dependency on conventional energy sources and promoting eco-friendly agricultural practices. Successful implementation highlights its potential as a viable and sustainable solution to address farmers' energy and water scarcity challenges, contributing to rural development and environmental conservation.

Keywords: PV, Grid-Interfaced, Water Pumping, ANFIS, MPPT.

Tob Regul Sci. ™ 2023;9(1): 3879-3890
DOI: doi.org/10.18001/TRS.9.1.272

I. Introduction

Access to reliable and sustainable water supply is crucial for agricultural activities, especially in rural and remote areas where electricity is scarce or unreliable. In recent years, a growing interest has been in utilizing renewable energy sources to power water pumping systems for sustainable agriculture. One such innovative solution is designing and implementing an intelligent grid-interfaced solar water pumping system [1].

The intelligent grid-interfaced solar water pumping system combines the benefits of solar photovoltaic (SPV) technology with intelligent grid integration to provide a cost-effective and efficient solution for agricultural water pumping. This system aims to address the challenges farmers face in remote areas by harnessing the sun's power and optimizing energy usage [2].

The proposed research paper focuses on designing and implementing this intelligent grid-interfaced solar water pumping system for sustainable agriculture. It aims to explore the various components, control strategies, and integration techniques involved in the system. The research paper also evaluates this system's economic and environmental advantages compared to traditional diesel generators.

The system can efficiently manage power flow, optimize performance, and ensure reliable water supply for agricultural needs by utilizing intelligent grid interfacing. Integrating solar energy reduces fossil fuel dependency, resulting in reduced carbon emissions and a more sustainable approach to water pumping in agriculture.

The research paper draws insights from existing studies [1-4] and proposes a comprehensive analysis of the intelligent grid-interfaced solar water pumping system. It aims to contribute to the existing body of knowledge by providing valuable insights into the design, implementation, and benefits of this system for sustainable agriculture. Overall, the research paper aims to serve as a valuable resource for researchers, engineers, policymakers, and farmers interested in sustainable water supply solutions for agriculture. It highlights the potential of intelligent grid-interfaced solar water pumping systems to revolutionize agricultural practices, improve productivity, and contribute to a more sustainable future.

II. Proposed System Design

A solar photovoltaic (PV) array, an induction motor drive, a voltage source inverter (VSI), a voltage source converter (VSC), and a boost converter for Maximum Power Point Tracking (MPPT) are the components that make up the suggested system. The configuration of the system that is being considered is depicted in Figure 1.

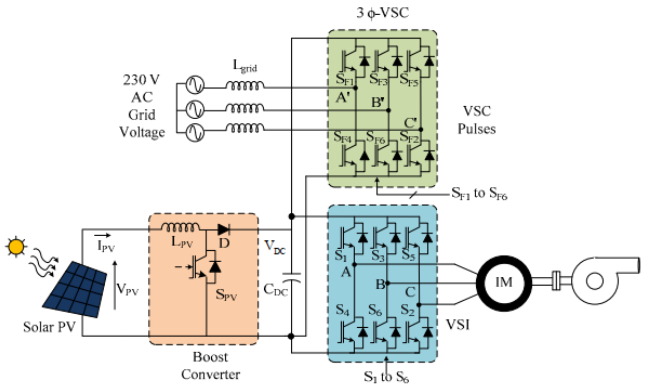

Fig. 1. **Schematic Representation of the Overall System Model.**

II.1 Modelling of PV array

PV is an area of technology and research related to devices that directly convert sunlight into electricity. Solar cells are an essential element of PV technology. Solar cells are made of semiconductor materials, such as silicon. One of the most valuable properties of semiconductors is that their conductivity can be easily modified by introducing a mixture into the crystal lattice.

This solar cell works because when a photon of light falls on the cell, the photon transfers energy to a charge carrier. The electric field across the junction separates the light-generated positive charge carriers (holes) from their negative counterparts (electrons). This way, an electric current is extracted after the circuit is closed on an external load [5]. The Single diode circuit model is among the most common models to predict PV cell energy production [6-8]. The parameters of the solar panels used in this system are presented in Table I.

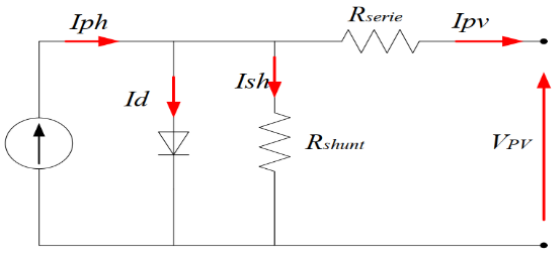

Fig. 2. **Equivalent circuit of a PV cell.**

TABLE 1. ELECTRICAL CHARACTERISTICS OF THE PV MODULE.

Solar Photovoltaic Module	
DESCRIPTION	RATING
Cell	60
Open circuit voltage (Voc)	35.7 V
Short circuit current (Isc)	7.99 A
Voltage at Maximum Power (Vmp)	28.7 V
Current at Maximum Power (Imp)	7.32 A
Solar Photovoltaic Array	
Maximum power (Pmax)	2.3 KW
Voltage, Vmpp	315.7 V
current, Impp	7.32 A
Modules number at series, Ns	11
Modules number at parallel, Np	1

The I-V and P-V characteristics against different radiation levels through simulation are shown in Fig. 3:

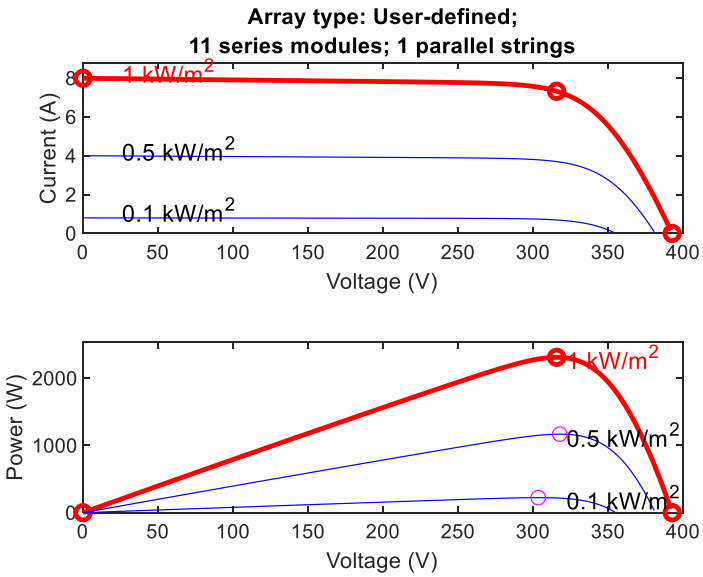

Fig.3. I-V and P-V characteristics of PV array.

II.2 Design of Boost DC-DC Converter

SPV matrix voltage MPP, Vpv= Vmpp= 315.7 V, is increased with VSI voltage DC bus, Vdc= 400 V. These present a minimal working ratio, D, which outcomes in an advantage mentioned in section earlier. Table II summarises the estimation of inductance, L, and capacitance, C, where fsw is the boost converter's switch frequency, IL is the inductor's current, and IL is the ripple content at the inductor's current inductance [9,10].

TABLE 2. BOOST DC-DC CONVERTER PARAMETERS.

Parameter	Value
D	0.23
L	3 mH
C	500 uF
IL	4.75 A
Δ IL	10% of IL
fsw	10 kHz

II.3 Induction Motor

In the (α, β) reference frame, the dynamic behavior of a three-phase induction motor appears as follows [11]:

The stator voltages:

$$\begin{cases} V_{s\alpha}=R_s I_s+\dfrac{d\phi_{s\alpha}}{dt} \\ V_{s\beta}=R_s I_s+\dfrac{d\phi_{s\beta}}{dt} \end{cases}$$

The rotor voltages:

$$\begin{cases} O=R_r I_{r\alpha}+\dfrac{d\phi_{r\alpha}}{dt}+\omega_m\phi_{r\beta} \\ O=R_r I_{r\beta}+\dfrac{d\phi_{r\beta}}{dt}+\omega_m\phi_{r\alpha} \end{cases} \quad (2)$$

The stator flux:

$$\begin{cases} \phi_{s\alpha}=L_s I_{s\alpha}+MI_{r\alpha} \\ \phi_{s\beta}=L_s I_{s\beta}+MI_{r\beta} \end{cases} \quad (3)$$

The rotor flux:

$$\begin{cases} \phi_{r\alpha}=L_r I_{r\alpha}+MI_{s\alpha} \\ \phi_{r\beta}=L_r I_{r\beta}+MI_{s\beta} \end{cases} \quad (4)$$

The electromagnetic torque:

$$Te=\frac{3}{2}\times p\left(I_{s\beta}\phi_{s\alpha}-I_{s\alpha}\phi_{s\beta}\right) \quad (5)$$

Where, $I_{s\alpha}$, $I_{s\beta}$, $I_{r\alpha}$, and $I_{r\beta}$ are the (α-β) frame stator and rotor currents; M is the mutual inductor; L_s, L_r, R_s, and R_r are the stator and rotor inductors and resistors.

II.4 Centrifugal Pump

Equation (6) demonstrates that the centrifugal pump load torque (Tpump), is related to the square of the induction motor speed (Ω) [12].

$$T_{pump} = K_{pump}\Omega^2 \quad (6)$$

Where, K_{pump} is the centrifugal pump's constant.

III. Control Of The Proposed System

The diagram in Figure 4 illustrates the management of the system. The system receives power from two sources: the SPV array and the utility grid supply. The control mechanism is specifically designed to intelligently distribute and utilize the available power from both sources. Moreover, the system is engineered to adapt to variations in radiation and environmental conditions, ensuring its resilience.

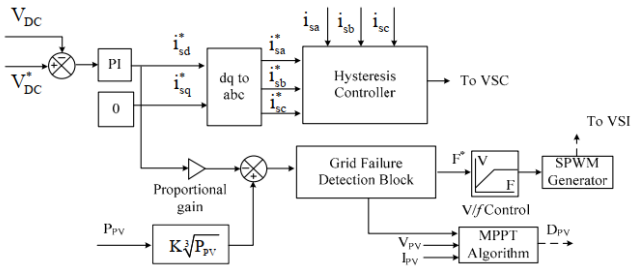

Fig. 4. The proposed intelligent solar water pumping system management.

The system operates in three different modes to effectively utilize solar power and grid supply while maintaining the rated pump discharge.

Mode I: In this mode, only solar power is available, and the grid supply is absent. If the available solar power exceeds the pump's rated power, the pump runs at its maximum capacity. In this case, the Maximum Power Point Tracking (MPPT) algorithm is not active. However, if the available solar power is less than the pump's rated power, the reference frequency for the pump is estimated based on the maximum available solar power.

Mode II: This mode operates when there is no solar power available, such as during the night or low solar radiation. The system is then powered solely by the single-phase grid supply, maintaining the rated speed and discharge. To improve the power quality from the grid, a single-phase two-level voltage source converter (VSC) is employed.

Mode III: During the daytime when there is sufficient solar insolation and the grid supply is available, the system combines power from both sources to meet the required pump discharge. The output power from the solar photovoltaic (SPV) array varies throughout the day due to changes in weather, sun position, panel orientation, and shadows from nearby objects. The excess power, if any, can be obtained from the grid. Additionally, a front-end converter is used to ensure that the total harmonic distortion (THD) of the AC mains remains within acceptable limits.

IV. MPPT Algorithm

Figure 5 depicts the proposed ANFIS (Adaptive Neuro-Fuzzy Inference System) power-voltage controlled MPPT (Maximum Power Point Tracking) controllers. In this MPPT configuration, a replicated model of the solar PV system is constructed using ANFIS. The ANFIS is trained with two inputs, namely irradiance and temperature, and a single output, which represents power under different irradiance and temperature conditions. The power reference obtained from the ANFIS system is then compared with the actual PV power. Any difference, or error power, is processed through a proportional-integral controller to generate a reference voltage for the subsequent stage.

In the next stage, the reference voltage is compared with the actual PV voltage, resulting in an error voltage. This error voltage is further processed through another proportional-integral controller, which ultimately provides the duty cycle for the Pulse Width Modulation (PWM) generator. The PWM generator generates pulses for the DC-DC boost converter, ensuring the maximum power extraction from the solar PV array.

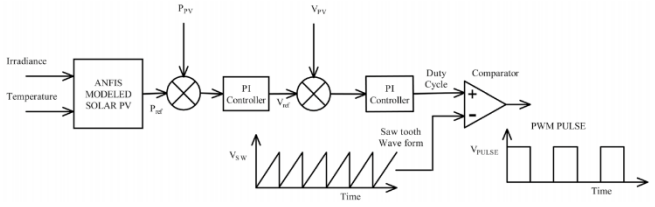

Fig 5. The ANFIS-based power-current controlled Maximum Power Point Tracking (MPPT) system.

V. Induction Motor Control

Due to the fact that the pump utilizes a centrifugal principle for operation, there is a correlation between the speed of the IMD and the amount of water that is expelled from the pump. The volts per Hertz (V/f) control approach is utilized in order to maintain a constant speed for the IMD.

To avoid dangerously high starting currents, the IMD is started with a procedure known as a soft start. The control logic shown in Figure 2, which is used to determine the frequency reference, is shown below. The proposed system always runs at its rated speed while it is under normal conditions, except for situations in which the grid is not present and the maximum power that is available is less than the IMD's rated power.

The voltage of the DC link is kept under control by a proportional-integral (PI) controller. The error that was produced by the PI controller is utilized in the calculation of the reference current (i_s^*), which is then compared with the supply current that was sensed. To generate switching pulses for the front-end converter, the output of this comparison is sent into a hysteresis current controller.

In addition to that, the output of the PI controller is sent into a proportional controller as well. The output of the proportional controller is subtracted from the feed-forward term ω_1^*, which is obtained from the power output of the PV modules, and the result is denoted by F^*. The value of F^* is then sent to the V/f block, which is responsible for determining the switching pulses for the VSI (Voltage Source Inverter).

The expression for the speed term that corresponds to the PV power is as follows:

$$\omega_1^* = K_{pump}\sqrt[3]{P_{pv}}$$

The reference speed of the IMD, denoted by the notation F*, is determined by applying the following formula:

$$\omega^* = \frac{\omega_1^* - \omega_p}{2\pi}$$

VI. Simulation And Results

1. The System's Performance While Running in Mode I

Figures 6-9 depict the performance of the system in Mode I, where only solar PV drives the pump. The steady-state characteristics of the system are shown in these figures. Figure 6 shows that VPV and IPV are maintained at their MPP values. Additionally, the DC link is maintained at the reference voltage of 400V, as shown in Figure 8. The induction motor currents maintain sinusoidal waveshape, and the torque and speed of the motor are constant at the value corresponding to the radiation of 1000 W/m2, as shown in Figure 7. Figure 9 illustrates that the grid supply is absent.

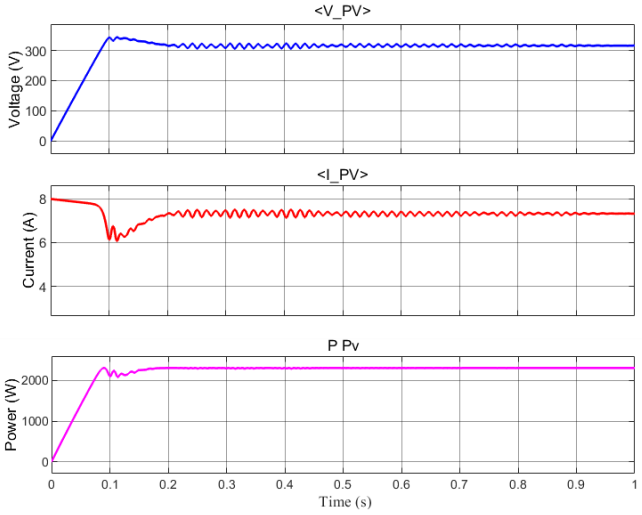

Fig .6. The simulation results of mode I of output voltage, curren, and output power of the PV.

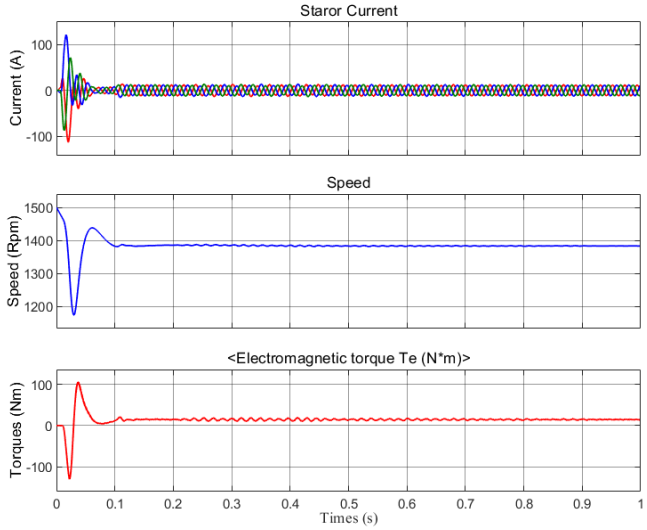

Fig.7.The simulation results of induction motor currents, the torque, and speed of the motor in mode I.

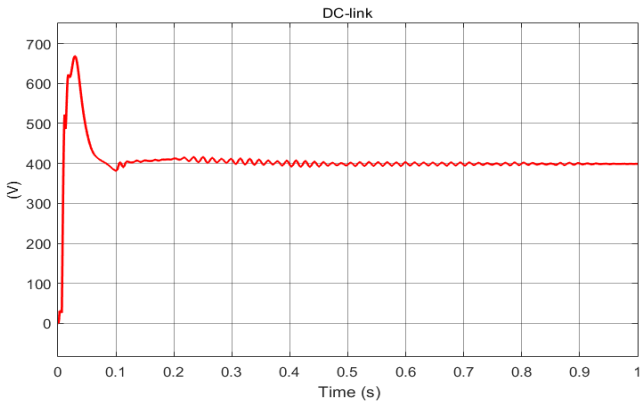

Fig.8. DC Link voltage in mode I.

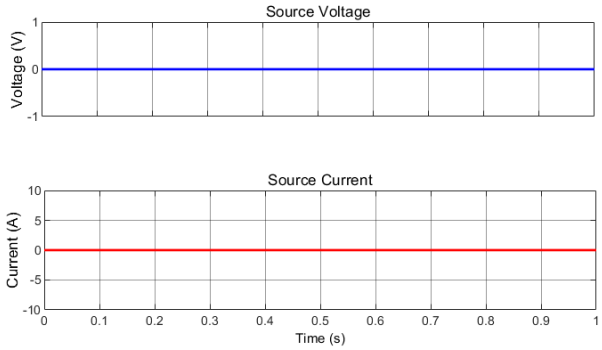

Fig.9. Grid side voltage and current waveforms of mode I.

2. The System's Performance While Running in Mode II

Figures 10-13 display the performance of the system operating in mode II, where the grid supply solely powers the drive. The input current remains in phase with the input voltage, ensuring the total harmonic distortion remains below 5%.

The DC link voltage is consistently maintained at the reference value of 400V, as depicted in Figure 12. Additionally, Figure 13 illustrates the grid's capability to cover the power demands, enabling the grid current to reach 15 amperes for effectively powering the motor.

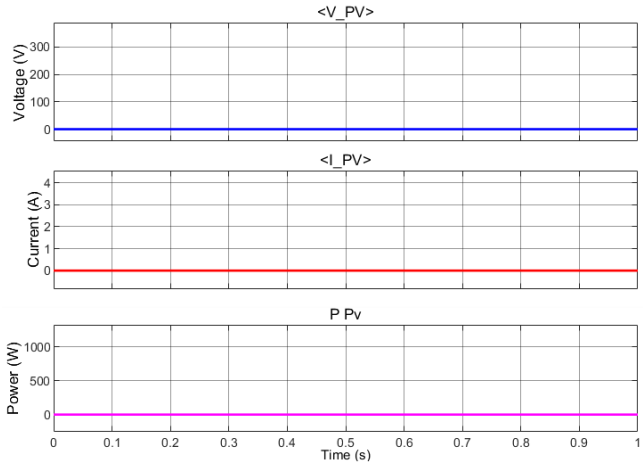

Fig.10. The simulation results of mode II of output voltage, curren, and output power of the PV.

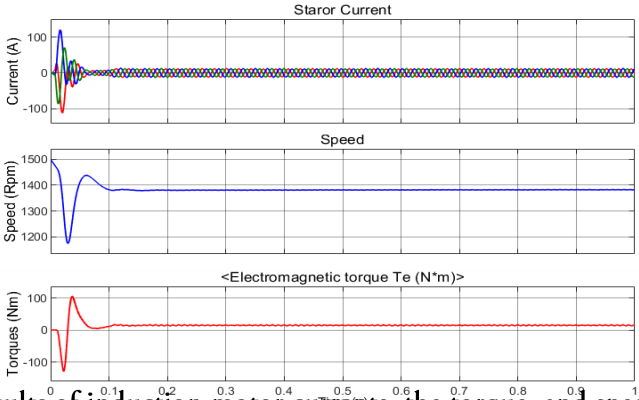

Fig.11. The simulation results of induction motor currents, the torque, and speed of the motor in mode II.

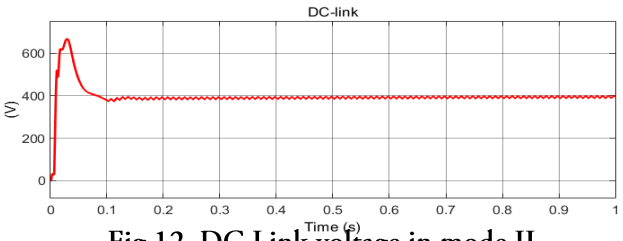

Fig.12. DC Link voltage in mode II.

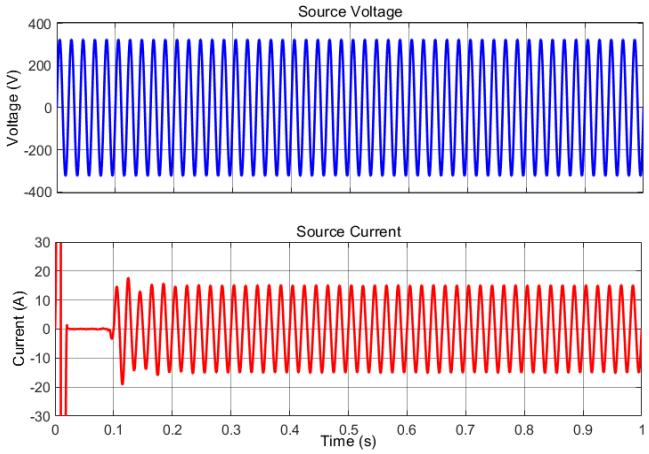

Fig.13. Grid side voltage and current waveforms of mode II.

3. The System's Performance While Running in Mode III

The system's dynamic performance in mode III is illustrated in Figures 14-17. The figures show the variation of the system indices with a decrease in radiation from 500 W/m^2 to 0 W/m^2, then a step change in radiation from 0 W/m^2 to 300 W/m^2, with available the grid supply.

The Ipv and Ppv decrease with the decrease in radiation as shown in Fig. 14. However, the induction motor currents, speed of the motor, and torque are maintained despite the decrease in radiation due to the presence of the grid utility in the service space. The grid covers the missing energy from the PV panels, as shown in Figures 15 and 17. The DC link is maintained at the reference voltage of 400V, as shown in Figure 16. Figure 17 illustrates that the grid current changes inversely with the solar panel current, increasing in the absence of energy extracted from the solar panels.

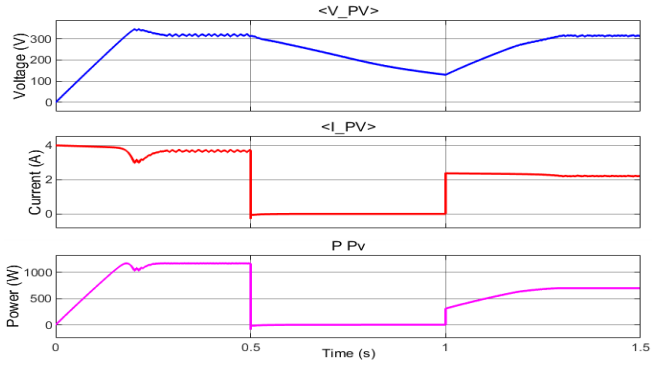

Fig.14. The simulation results of mode III of output voltage, curren, and output power of the PV.

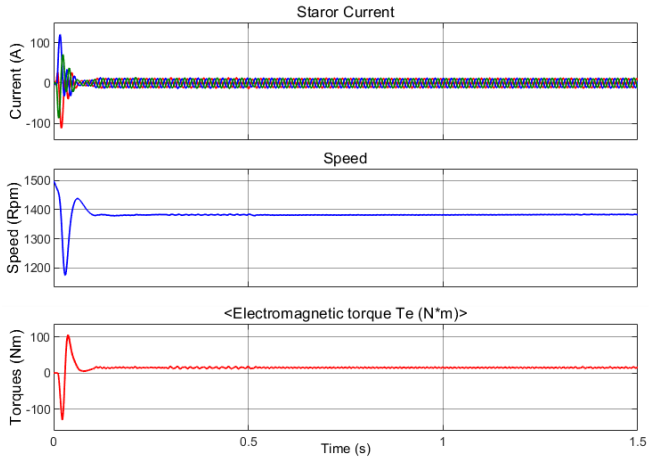

Fig.15.The simulation results of induction motor currents, the torque, and speed of the motor in mode III.

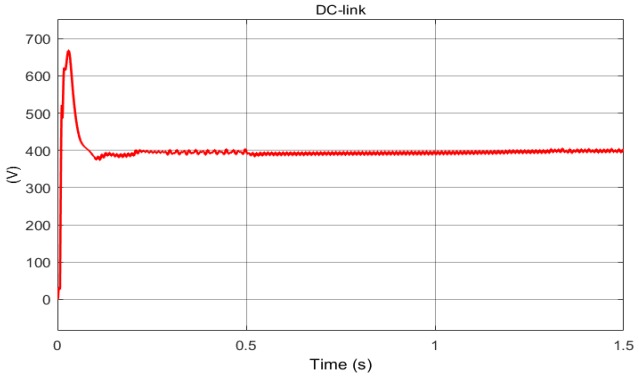

Fig.16. The DC Link voltage in mode III.

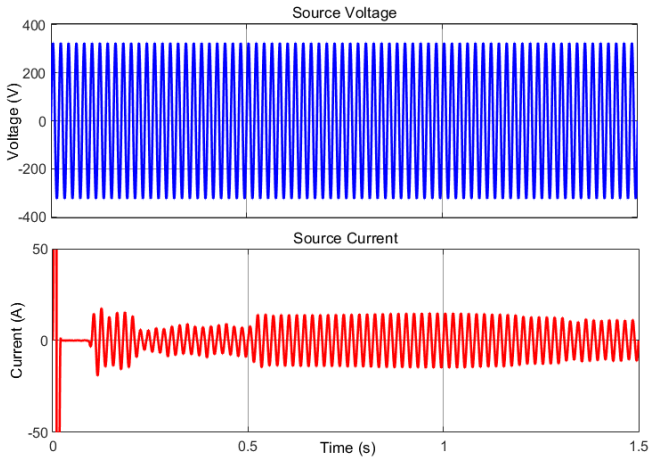

Fig.17. Grid side voltage and current waveforms of mode III.

VII. Conclusion

This research paper comprehensively investigates an innovative Intelligent Grid Interfaced Solar Water Pumping System for Sustainable Agriculture, utilizing an ANFIS-based MPPT algorithm. The study aims to enhance energy efficiency by harnessing solar energy for water pumping. The ANFIS algorithm demonstrated adaptability and accuracy in tracking the solar

array's maximum power point, increasing energy utilization. Integration with the power grid allows surplus energy injection, promoting sustainability. Successful implementation highlights its potential as a viable solution for agriculture's energy and water scarcity challenges, fostering eco-friendly practices and rural development. The research provides valuable insights for integrating ANFIS-based MPPT into various renewable energy systems, paving the way for a greener and more sustainable future.

References

[1] U. Sharma, B. Singh, and S. Kumar, "Intelligent grid interfaced solar water pumping system," *IET Renew. Power Gener.*, vol. 11, no. 5, pp. 614–624, Apr. 2017, doi: 10.1049/IET-RPG.2016.0597.

[2] T. K. S and S. K. Mittal, "Intelligent Grid Connected Solar Water Pumping Scheme , Using BLDC Drive," vol. 8, no. 2, pp. 450–458, 2021.

[3] R. C. Ilambirai, S. Ramasamy, and N. Hari, "Review of Special Electric Drives aided Photovoltaic Pumping and Proposal of a New Hybrid Grid Interactive Water Pumping System," *Int. J. Renew. Energy Res.*, vol. 12, no. 1, pp. 320–338, 2022, doi: 10.20508/IJRER.V12I1.12708.G8407.

[4] U. Sharma, B. Singh, and S. Kumar, "Intelligent grid interfaced solar water pumping system," *Iet Renew. Power Gener.*, vol. 11, no. 5, pp. 614–624, Apr. 2017, doi: 10.1049/IET-RPG.2016.0597.

[5] M. Y. Dennai, H. Tedjini, A. Nasri, and D. Taibi, "MPC controller of PV system based Three-Level NPC Inverter under different climatic conditions connected to the grid," *Prz. Elektrotechniczny*, vol. 97, no. 3, pp. 130–137, 2021, doi: 10.15199/48.2021.03.25.

[6] K. Ishaque, Z. Salam, and H. Taheri, "Accurate MATLAB simulink PV system simulator based on a two-diode model," *J. Power Electron.*, vol. 11, no. 2, pp. 179–187, 2011, doi: 10.6113/JPE.2011.11.2.179.

[7] R. M. da Silva and J. L. M. Fernandes, "Hybrid photovoltaic/thermal (PV/T) solar systems simulation with Simulink/Matlab," *Sol. Energy*, vol. 84, no. 12, pp. 1985–1996, Dec. 2010, doi: 10.1016/J.SOLENER.2010.10.004.

[8] R. V. Dell'Aquila, L. Balboni, and R. Morici, "A new approach: Modeling, simulation, development and implementation of a commercial grid-connected transformerless PV inverter," *SPEEDAM 2010 - Int. Symp. Power Electron. Electr. Drives, Autom. Motion*, pp. 1422–1429, 2010, doi: 10.1109/SPEEDAM.2010.5542040.

[9] B. Singh and R. Kumar, "Simple brushless DC motor drive for solar photovoltaic array fed water pumping system," *IET Power Electron.*, vol. 9, no. 7, pp. 1487–1495, Jun. 2016, doi: 10.1049/IET-PEL.2015.0852.

[10] M. Potok, "Microwave Devices and Circuits," *Electron. Power*, vol. 26, no. 7, p. 592, 1980, doi: 10.1049/EP.1980.0308.

[11] M. Errouha, A. Derouich, S. Motahhir, O. Zamzoum, N. El Ouanjli, and A. El Ghzizal, "Optimization and control of water pumping PV systems using fuzzy logic controller," *Energy Reports*, vol. 5, pp. 853–865, Nov. 2019, doi: 10.1016/J.EGYR.2019.07.001.

[12] A. Saoudi, S. Krim, and M. F. Mimouni, "Enhanced intelligent closed loop direct torque and flux control of induction motor for standalone photovoltaic water pumping system," *Energies*, vol. 14, no. 24, 2021, doi: 10.3390/en14248245.